Available online at www.sciencedirect.com
ScienceDirect
Thermochimica Acta 451 (2006) 139–148
thermochimica acta
www.elsevier.com/locate/tca

Reaction-diffusion model for the reaction bonding of alumina–zirconia composites using the intermetallic compound $ZrAl_3$

H. Geßwein*, J.R. Binder, H.-J. Ritzhaupt-Kleissl, J. Haußelt

Forschungszentrum Karlsruhe, Institut für Materialforschung III, Postfach 3640, 76021 Karlsruhe, Germany

Received 3 April 2006; received in revised form 1 September 2006; accepted 8 October 2006
Available online 13 October 2006

Abstract

This paper describes a reaction-diffusion model for the reaction of a gaseous oxidant (O_2) and a reactive solid ($ZrAl_3$), which allows for the consumption of the solid and the oxidant. The experimentally determined "kinetic triplet" (i.e. Arrhenius parameters E_a and A and the reaction model $f(\alpha)$) for the oxidation of $ZrAl_3$ powders is incorporated in the model, which consists of simultaneous mass and energy balances. The resulting system of partial differential equations is solved with the numerical method of lines for the 1D case. The influence of different processing parameters is studied and the numerical results are compared with experimental thermogravimetric data. The model is used to find optimal heating cycles for the production of defect-free reaction bonded alumina–zirconia composites of different sizes and to avoid uncontrollable thermal runaway reactions.
© 2006 Elsevier B.V. All rights reserved.

Keywords: Kinetics; Oxidation; Firing; Thermogravimetric analysis; Simulation

1. Introduction

Reaction bonding techniques such as the reaction bonding of aluminum oxide (RBAO) or the reaction bonding of silicon nitride (RBSN) are alternative ceramic processing methods offering various advantages over conventional processing routes. These advantages include the near-net shape capability which makes these techniques suitable for the manufacture of complex shapes produced by either slip casting, injection moulding or machining of green bodies [1]. The processes are based on the heterogeneous gas–solid reaction of a metal in an oxidizing atmosphere. Gas–solid reactions are usually extremely exothermic and result in a volume expansion. Therefore reaction control is essential for the production of high quality reaction bonded ceramics and to avoid typical process problems like cracking and bloating of the green powder compacts.

The use of intermetallic compounds in the systems Zr–Al and Zr–Si offers the advantage of a much higher volume increase during oxidation compared to pure metals like aluminum or silicon [2,3]. Reaction bonded alumina–zirconia composites with low sintering shrinkage can be produced by the reaction of a $ZrAl_3$ green body with an oxygen-containing atmosphere according to the following reaction scheme:

$$ZrAl_{3(s)} + \tfrac{13}{4}O_{2(g)} \longrightarrow ZrO_{2(s)} + \tfrac{3}{2}Al_2O_{3(s)} \quad (1)$$

This oxidation reaction is extremely exothermic ($\Delta H = -19.76\,\mathrm{kJ/g}$) [4,5] and uncontrolled reaction behavior may occur which can lead to local overheating and cracking of the green body.

Different modelling approaches for the RBSN [6,7] or RBAO processs [8–10] can be found in literature. The current study presents a reaction-diffusion model for the reaction bonding of alumina–zirconia composites based on the oxidation of the intermetallic compound $ZrAl_3$. The developed model incorporates an experimentally determined rate law for the oxidation of $ZrAl_3$ powders and a phenomenological description of oxygen diffusion and consumption in the porous green body. The material balances are coupled with an overall energy balance to account for heat generation from the chemical reaction and heat losses due to convection and radiation. The aim of this study is to investigate the influence of different processing parameters like sample size and heating cycle on the reaction behavior of $ZrAl_3$ green compacts.

* Corresponding author. Tel.: +49 7247 82 4055; fax: +49 7247 82 4612.
E-mail address: holger.gesswein@imf.fzk.de (H. Geßwein).

0040-6031/$ – see front matter © 2006 Elsevier B.V. All rights reserved.
doi:10.1016/j.tca.2006.10.004

2. Experimental

To compare the numerical results with experimental measurements, cylindrical green compacts measuring 5.9 mm in diameter and approximately 3.5 mm in length were prepared by uniaxial pressing ball milled $ZrAl_3$ powder (Alfa Aesar, 99%, metals basis) at a pressure of 300 MPa. A more detailed description of the powder preparation can be found elsewhere [11]. Weight changes which occured during reaction sintering were monitored by thermogravimetry (Netzsch STA 449C). The oxidations were performed under artificial air (20.5% O_2 in N_2) at a gas flow in the thermal analyzer of 50 ml/min. The samples were placed on small alumina crucible lids inside the TG/DSC analyzer. The specific heat was determined by DSC measurements (Netzsch DSC 404C) and the thermal diffusivity was measured using the laser flash method (Netzsch LFA 427). The diameter and height of the cylindrical $ZrAl_3$ green bodies were measured with a micrometer screw. Green densities were calculated from weight and geometry of the samples. Pore sizes were estimated from Hg-porosimetry measurements (Porotec Pascal 140/440) and the porosity is calculated from the geometrical density. Ignition measurements were conducted in a box furnace where two additional type S thermocouples were attached to uniaxial compacted cylindrical samples (diameter 5.9 mm and approximately 5 mm long) to measure the temperature both of the sample and near the sample surface. The output from each thermocouple was recorded using a PC.

3. Reaction-diffusion model

3.1. Model development

The reaction of a porous reactive solid and a gaseous oxidant can be described with reaction-diffusion models [12,13], where the consumption of the solid and the gas, as well as the diffusion of the gas through the porous matrix are included. In the following a one-dimensional model for a cylindrical sample of diameter d and length $2L$ which is surrounded by a reservoir of constant gas-phase concentration is developed. Only the spatial coordinate corresponding to the cylindrical axis is considered. Such one-dimensional approximations of reaction-diffusion systems were studied by Mercer and coworkers [14–17] and were succesfully used to model the combustion synthesis of intermetallic compounds [18–20]. Fig. 1 shows the schematic geometry with the spatial coordinate system. For simplicity various restrictive assumptions were made:

(1) The unreacted and oxidized material have the same physical characteristics, i.e. thermal conductivity, heat capacity and the pore structure of the solid remain constant during the reaction.
(2) The dependence of the temperature and the relative concentrations from other spatial coordinates has been neglected and thus oxygen diffusion from the surrounding into the medium is confined to the base planes of the cylindrical sample.
(3) As a first approximation the overall reaction rate r is assumed to be of first order in the oxygen concentration (see Section 3.2). Thus, the $ZrAl_3$–O_2 reaction takes place whenever the concentration functions C_{ZrAl_3} and C_{O_2} are simultaneously different from zero. Within this asumption the consumption of oxygen in the void space is taken into account, but it has to be mentioned that this expression is empirical and does not attempt to describe the exact influence of the oxygen partial pressure on the reaction mechanism.

3.2. Oxidation kinetics

The rate of solid-state or heterogeneous processes can be generally described by

$$\frac{d\alpha}{dt} = k(T)f(\alpha) = A\ \exp\left(-\frac{E_a}{RT}\right) f(\alpha) \tag{2}$$

where $f(\alpha)$ is a function of the degree of conversion, t the time, T the temperature, $k(T)$ the rate constant, A the pre-exponential factor, E_a the apparent activation energy and R is the gas constant. If gaseous reactants or products are involved in the reaction, a function of their concentrations $f_2(C_i)$ is included in Eq. (2). The functions $f(\alpha)$ and $f_2(C)$ originate from physico-geometric considerations and/or the law of mass action. For examples of the most common $f(\alpha)$ functions used in heterogeneous kinetics, see Brown et al. [21].

The oxidation kinetics of $ZrAl_3$ powders were studied in detail in a previous paper [11]. In that study thermogravimetry was used to determine the kinetic parameters. The oxidation process could be well described by a generalized n-dimensional Avrami type rate equation (A_n) of the form $f(\alpha) = n(1-\alpha)[-\ln(1-\alpha)]^{1-1/n}$, which is a formal kinetic law and generally applies

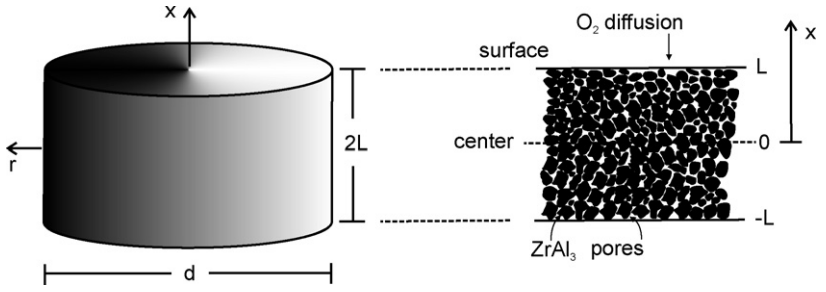

Fig. 1. Schematic of the reacting sample used in the model.

for random nucleation and growth. The calculated apparent activation energy was 244 kJ/mol with a pre-exponential factor $\ln(A/s^{-1}) = 9.45$ and a kinetic exponent $n = 0.34$. This value of the Avrami exponent is relatively close to 0.5 and indicates a diffusion-limited process. The $A_{0.5}$ model corresponds to a nuclei growth model, where all nuclei are initially present and the growth process is one-dimensional with diffusion-control [22]. This is in accordance with the fact that the $ZrAl_3$ particles are initially covered with a thin oxide film. During oxidation the growth process continues inwards towards the center of the particles. The kinetic model is a formal kinetic description of the oxidation process and is valid only for the investigated $ZrAl_3$ powder, i.e. particle size and morphology and temperature and pressure conditions.

To account for the oxygen consumption in the reactive green body, the dependence of the overall oxidation rate r on the concentration of oxygen is assumed to be of the form $f_2(C_g) = C_g$, where C_g is the relative concentration of oxygen. The degree of reaction α is transformed into the relative concentration of the solid reactant $ZrAl_3$ by $C_s = 1 - \alpha$. Thus, a phenomenological expression for the overall reaction rate, r, can be written as follows:

$$r = A \exp\left(-\frac{E_a}{RT}\right) n C_s[-\ln(C_s)]^{1-1/n} C_g \tag{3}$$

This overall rate describes the oxidation of compacted $ZrAl_3$ samples and includes the microkinetics at the powder particle level ($f(C_s)$) as well as the influence of oxygen ($f_2(C_g)$) which has to diffuse into the sample to be available for the reaction.

The diffusion of oxygen through the porous solid is assumed to take place within the range defined by the Knudsen diffusion, which is a valid approximation for pore sizes of the solid matrix smaller than the mean free path of the diffusing gas molecules. Then the effective diffusivity of oxygen, D_{e,O_2}, is given as [9,23]:

$$D_{e,O_2} = \frac{\epsilon_s D_{O_2}}{\tau} \tag{4}$$

$$D_{O_2} = \frac{4}{3} r_p \left[\left(\frac{2}{\pi}\right)\left(\frac{RT}{M_{O_2}}\right)\right]^{1/2} \tag{5}$$

where ϵ_s is the internal void fraction, D_{O_2} the diffusivity of oxygen gas through the pore system, τ the tortuosity, r_p the pore radius and M_{O_2} is the molecular weight of oxygen.

3.3. Simultaneous mass and energy balance

The governing equations for a one-dimensional reaction-diffusion system including volumetric heat loss, which is an approximation to a two-dimensional system (a cylinder or a slab) where there is heat transfer at the boundaries (the circumference of the cylinder or the upper and lower surfaces of the slab) are given by [24]:

$$(1-\epsilon_s)\rho_s c_p \frac{\partial T}{\partial t} = k\frac{\partial^2 T}{\partial x^2} + (1-\epsilon_s)\rho_s Q r - \frac{4}{d}[h(T - T_a) + \sigma\epsilon(T^4 - T_a^4)] \tag{6}$$

$$\frac{\partial C_g}{\partial t} = D_e \frac{\partial^2 C_g}{\partial x^2} - \gamma r \tag{7}$$

$$\frac{\partial C_s}{\partial t} = -r \tag{8}$$

in which T is the temperature, r the overall reaction rate and C_g and C_s are the relative concentrations of oxygen and $ZrAl_3$, respectively. The last term on the right-hand side of Eq. (6) represents volumetric convective and radiative heat loss to the surroundings throughout the medium.

The other quantities appearing in (6)–(8) are defined in Table 1. The boundary conditions for the temperature and relative oxygen concentration are:

$$\frac{\partial T}{\partial x}(0,t) = 0 \tag{9}$$

$$\frac{\partial T}{\partial x}(L,t) = \frac{h}{k}(T_a(t) - T(L,t)) + \frac{\sigma\epsilon}{k}(T_a^4(t) - T^4(L,t)) \tag{10}$$

$$\frac{\partial C_g}{\partial x}(0,t) = 0 \tag{11}$$

$$\frac{\partial C_g}{\partial x}(L,t) = \frac{k_g}{D_e}(C_{g,a} - C_g(L,t)) \tag{12}$$

with the initial conditions:

$$C_s(x,0) = 1.0, \qquad T(x,0) = T_0, \qquad C_g(x,0) = 1.0 \tag{13}$$

where T_a and T_0 are the ambient and starting temperatures, respectively. Different heating cycles and furnace temperatures can be investigated by expressing the ambient temperature $T_a = T_a(t)$.

3.4. Model parameters

The values of the model parameters appearing in the system of differential equations (6)–(8) were determined experimentally when possible and are listed in Table 1. The tortuosity, which describes the pore structure, was assumed to be 5, an approximation taken from the literature [9]. Changes in the pore structure during oxidation are neglected. This was verified experimentally by porosity measurements of samples which were oxidized at different temperatures. Pore closure and sintering does not start until temperatures of approximately 1200 °C have been reached. Values for the emissivity, heat and mass transfer coefficients were also estimated from the literature [10,25,26]. The density of oxygen ρ_g is given by the ideal gas law as $p_{O_2} M_{O_2}/RT$, where M_{O_2} and p_{O_2} are the molecular mass and partial pressure of oxygen, respectively. For atmospheric pressure ρ_g is 0.27 kg/m^3 (assuming p_{O_2} is 0.21×10^5 Pa).

3.5. Numerical solution

The system of partial differential equations (6)–(8) was solved with the numerical method of lines (MOL). The governing partial differential equations with boundary conditions were transformed into a system of ordinary differential equations using centered finite differences for the spatial derivatives [27]. The resulting set of ordinary differential equations was

Table 1
Values for model parameters used in the calculations

Quantity	Symbol	Value
Pre-exponential factor	A	$2.818 \times 10^9\ s^{-1}$
Activation energy	E_a	2.44×10^5 J/mol
Avrami-exponent	n	0.337
Heat of reaction	Q	19.76×10^6 J/kg
Gas constant	R	8314 J/kmol K
Density $ZrAl_3$	ρ_s	4117 kg/m^3
Density O_2	ρ_g	0.27 kg/m^3
Specific heat	c_p	1000 J/kg K
Conductivity	k	2 W/m K
Stefan–Boltzmann coefficient	σ	5.67×10^{-8} W/(m^2 K^4)
Emissivity	ϵ	Varied between 0 and 0.9
Heat transfer coefficient	h	Varied between 0 and 40 W/m^2 K
Molecular mass of O_2	M_{O_2}	32 g/mol
Pore radius	r_{pore}	100×10^{-9} m
Porosity	ϵ_s	0.39
Tortuosity	τ	5
Diameter	d	0.006 m
Mass transfer coefficient	k_g	Varied between 0.006 and 0.01 m/s
Ratio of densities	$\gamma = (1-\epsilon_s)\rho_s/\rho_g$	10,063

solved in FORTRAN using the stiff integrator `radau5` [28]. In the calculations the number of grid points was approximately 100. Higher values of the internal node points did not cause any change in the results.

4. Model predictions and discussion

Numerous calculations were performed to identify the effects of several processing parameters during oxidation of $ZrAl_3$ green bodies. In the following the effects of heat and mass transfer, different furnace heating cycles and sample size on the reaction behavior are reported and finally, the numerical results are compared with experimetally measured thermogravimetric data of cylindrical samples. Unless otherwise stated, a length $2L$ of 1.5 mm is assumed.

4.1. Effects of heat and mass transfer

Heat losses due to convection and radiation between the green compact and the surrounding air are described by the conductive heat transfer coefficient h and the emissivity ϵ. The transfer of oxygen from the surrounding into the porous green body is described by an overall mass transfer coefficient k_g. Because of unknown conditions such as air velocity at the sample surface in the used furnace and thermal analyzer, constant values for these parameters are used in the calculations, which are summarized in Table 2. Fig. 2 shows the simulated TG and temperature difference curves ($\Delta T = T_{average} - T_{furnace}$) for a heating rate of 2 °C/min. For low values of the heat loss parameters the heat liberated by the oxidation reaction exceeds the heat losses and increased reaction rates with steep ΔT peaks are observed. Ignition phenomena can be avoided by increasing the heat loss parameters. This can be achieved by higher gas flow rates, by diluting the reaction gas with an high-thermal-conductivity inert gas or by increasing the emissivity of the sample. Varying gas permeability of the $ZrAl_3$ samples can be simulated by changing the overall mass transfer coefficient k_g. As k_g is increased an oscillatory reaction behavior is observed. After the reaction is accelerated by a temperature rise due to self-heating, the rate slows down because the available oxygen in the pore network of the $ZrAl_3$ compact is consumed. When enough oxygen is diffused back into the sample the temperature and reaction rate rise again.

Table 2
Values of heat and mass transfer parameters used in the calculations

Case	Heat transfer coefficient, h (W/m^2 K)	Emissivity, ϵ	Mass transfer coefficient, k_g (m/s)
A1	15	0.3	0.006
A2	0	0.3	0.006
A3	40	0.3	0.006
B1	15	0.0	0.006
B2	15	0.6	0.006
B3	15	0.9	0.006
C1	15	0.3	0.002
C2	15	0.3	0.008
C3	15	0.3	0.012

4.2. Effect of the heating cycle

The effects of different linear heating rates and hold times at various temperatures on the predicted reaction behavior are shown in Fig. 3. The heating rates vary between 1 and 10 °C. Additionally hold times of 10 h at temperatures between 500 and 700 °C as well as holds of 5, 10 and 15 h at a temperature of 600 °C are investigated. As can be seen from Fig. 3(a) and (b) a heating rate of 1 °C leads to low ΔT values, i.e. the sample temperature is approximately equal to the furnace temperature. Different reaction behavior can be observed for the higher heating rates. Higher heating rates result in pronounced ΔT peaks and therefore a runaway reaction with uncontrollable reaction behavior and sample cracking is more likely to occur. The effects of varying the hold temperature and hold time is shown in Fig. 3(c) and (d). The heating cycles consist of a linear heating rate of 2 °C/min before and after the isothermal hold. The programmed final temperatures are in each case 1000 °C. For the low hold temperatures of 500 and 550 °C the weight gain due to oxidation prior and during the 10 h hold is about 15 and 25%, respectively. The higher the hold temperature and hold time are, the higher the fraction of solid $ZrAl_3$ oxidized in the isothermal part of the reaction is. After the hold an increase of the conversion degree can be observed, which corresponds to the linear increase of the reaction temperature to the final temperature of 1000 °C. At this temperature the oxidation is completed for each investigated heating cycle.

Therefore it follows that for a complete, kinetically controlled oxidation of the $ZrAl_3$ compacts with constant weight gain, a heating schedule with different linear heating rates is most effective. The heating rates have to be adjusted carefully to avoid

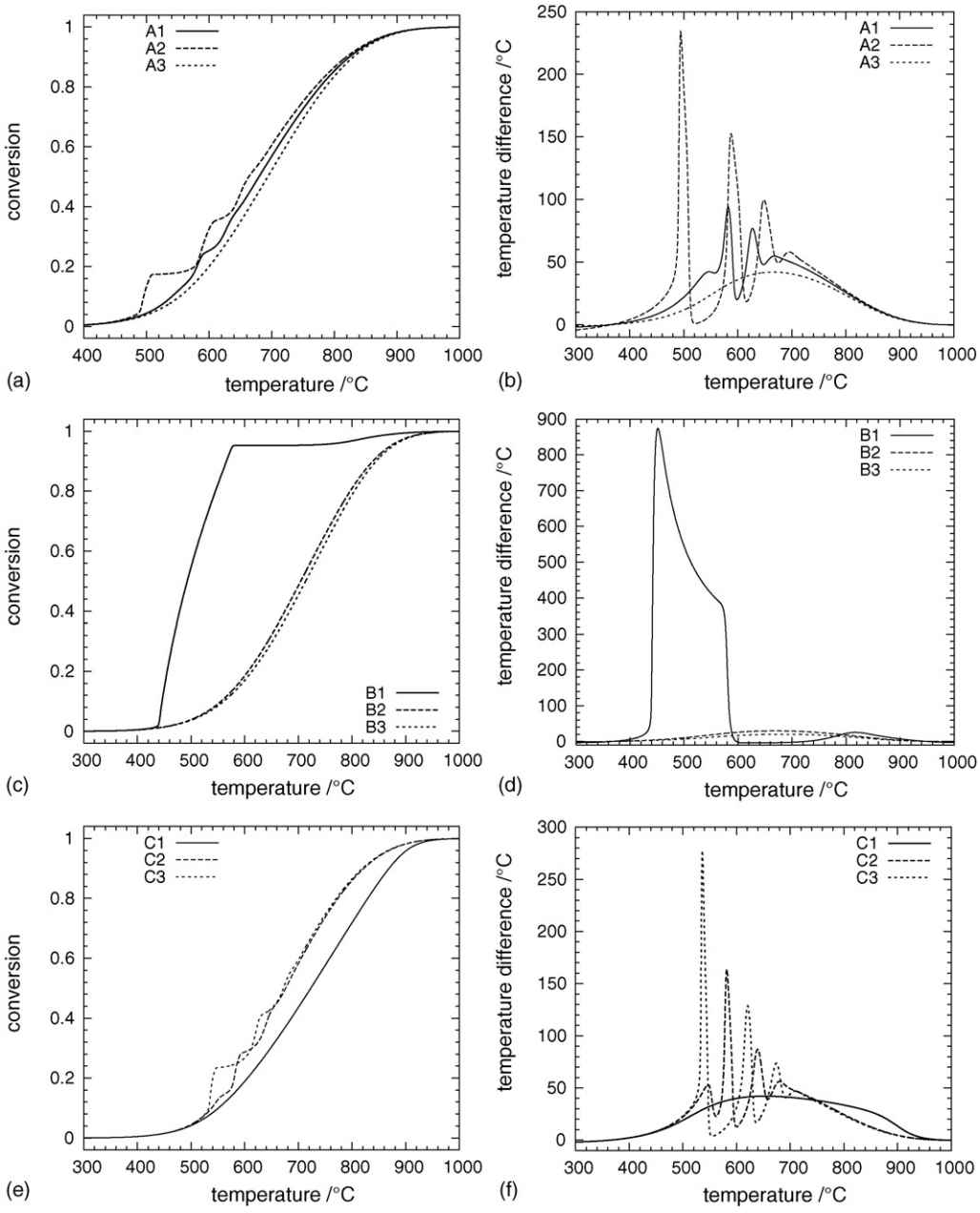

Fig. 2. Effects of heat and mass transfer on the model-predicted reaction behavior: (a and b) variation of h, (c and d) variation of ϵ and (e and f) variation of k_g.

runaway reactions depending on the temperature range and the sample size. This is demonstated in the next paragraphs.

4.3. Effect of the sample size

The oxidation process of $ZrAl_3$ compacts is controlled by the availability of oxygen. For loose powders and small sample sizes the diffusion paths for oxygen are small and there is always enough oxygen for the oxidation reaction available. In this borderline case the relative oxygen concentration remains almost constant and therefore the system of differential equations (6)–(8) can be reduced to the one-reactant system, i.e. only the $ZrAl_3$ concentration has to be considered. The effect of oxygen diffusion can be assessed by changing the sample size, i.e. changing the oxygen diffusion path lengths. The conversion curves for sample sizes L of 1.5, 3 and 6 mm are shown in Fig. 4. As is evident, the weight gain rate slows down as the sample size increases because of increasing oxygen diffusion path lenghts. In this case the overall reaction is diffusion-controlled. At atmospheric pressure the amount of gaseous oxygen in the pore network is not sufficient for a complete reaction and oxygen has to diffuse back from the surrounding into the porous matrix so that oxidation can continue. At a temperature of 1000 °C the 1.5 and 3 mm samples completely reacted, whereas the 6 mm sample only partially reacted. The lower reaction rates of the larger samples result in less pronounced broad ΔT peaks.

The effect of oxygen diffusion path lenghts on the reaction behavior can be clarified by the calculated $ZrAl_3$ conversion pro-

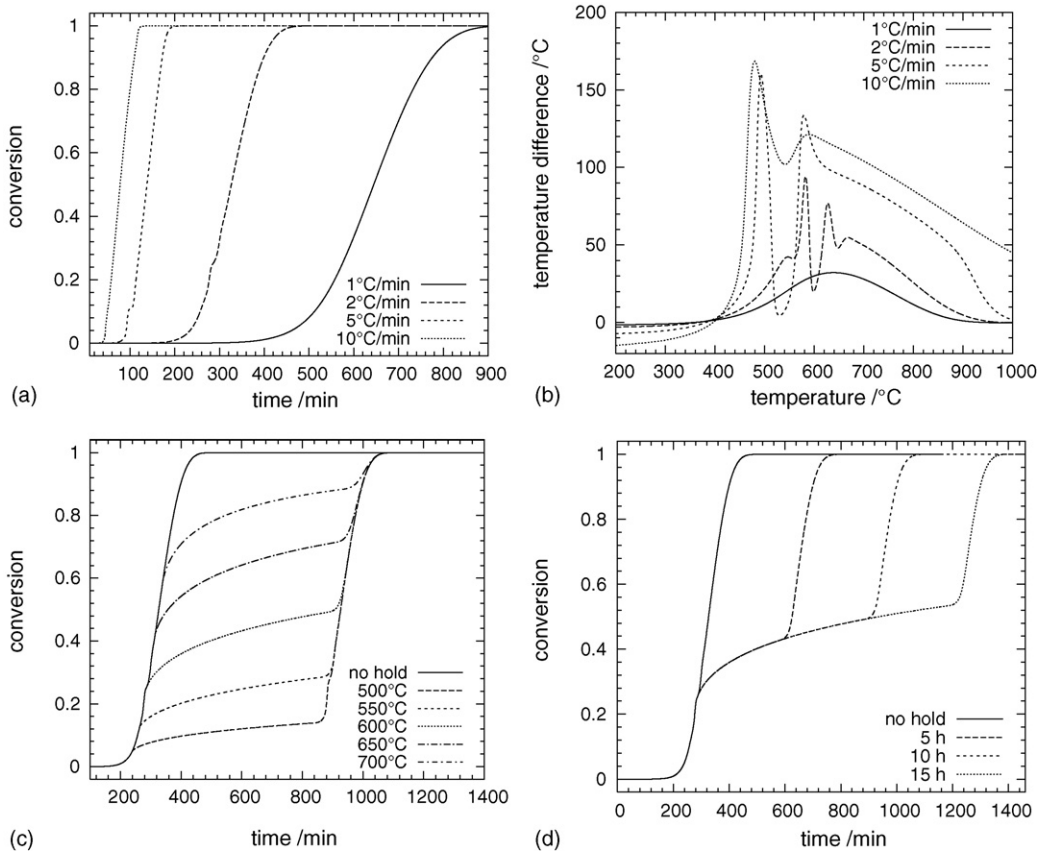

Fig. 3. Effect of different heating cycles on the reaction behavior of $ZrAl_3$ green bodies ($L = 1.5$ mm, $h = 15$ W/m^2 K, $\epsilon = 0.3$, $k_g = 0.006$ m/s). (a) Variation of the heating rate, (b) temperature difference curves for different heating rates, (c) effects of hold time of 10 h at different temperatures, and (d) effect of hold time at 600 °C (heating rates at (c and d) 2 °C/min).

files for the different sample sizes shown in Fig. 5. For a small sample size of $L = 1.5$ mm, the sample reacts uniformly and no gradient in the conversion profile can be observed whereas slight concentration gradients are developed during the oxidation of the 3 mm sample. For these smaller samples the rate determing step is the oxidation of the $ZrAl_3$ particles, which means that oxygen transport through the pore system is fast due to the short diffusion path lengths and oxygen is therefore available for reaction throughout the green body at all times. By contrast the oxidation of the large sample is mainly diffusion-controlled. As can be clearly seen in Fig. 5(c), after a short period of time steep gradients are developed in the conversion profiles. At higher temperatures oxygen is quickly consumed at the reaction front and the progress of the front is governed by the transport of oxygen through the pore system to the reaction front. The development of such steep composition gradients can lead to mechanical stresses in the reacting green compacts which can cause defects like cracks. To avoid these composition gradients

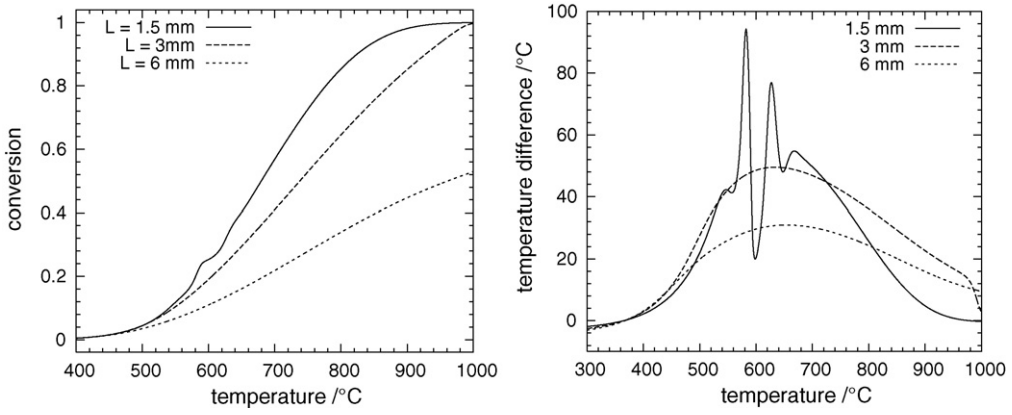

Fig. 4. Effect of sample size L on model-predicted mass gain of $ZrAl_3$ green bodies (left) and temperature difference curves (right).

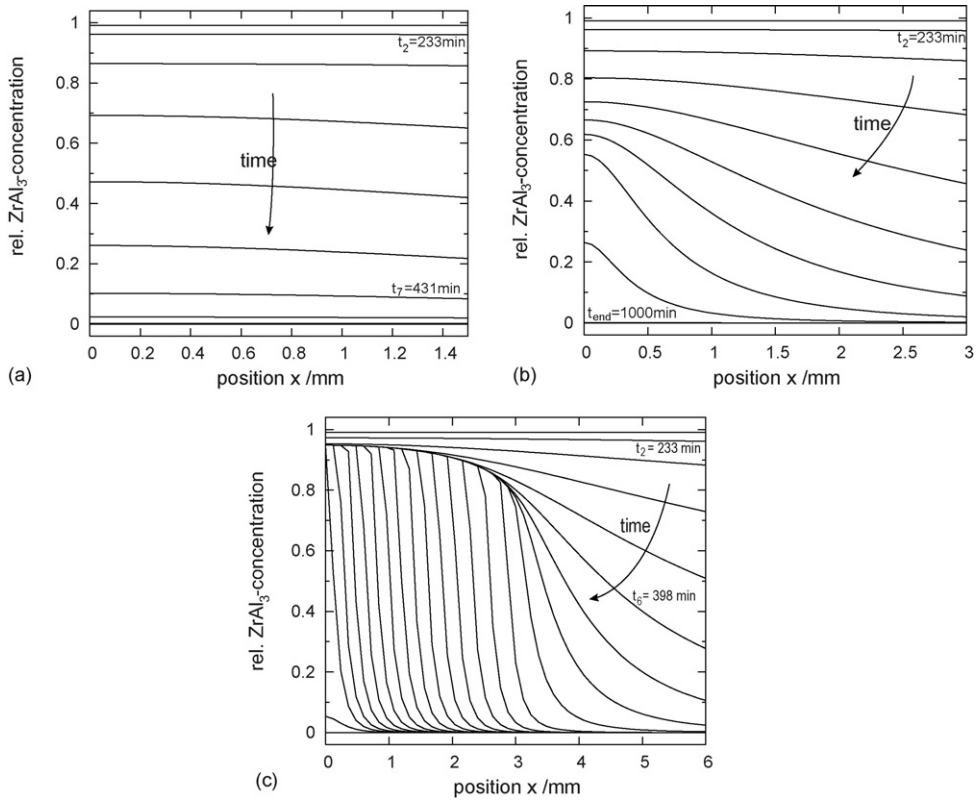

Fig. 5. Progression of the $ZrAl_3$ conversion profiles for (a) 1.5 mm, (b) 3 mm and (c) 6 mm samples with constant heating rate of 2 °C/min to 1000 °C and isothermal hold time; the time steps between the conversion profile curves are ∼33 min, respectively.

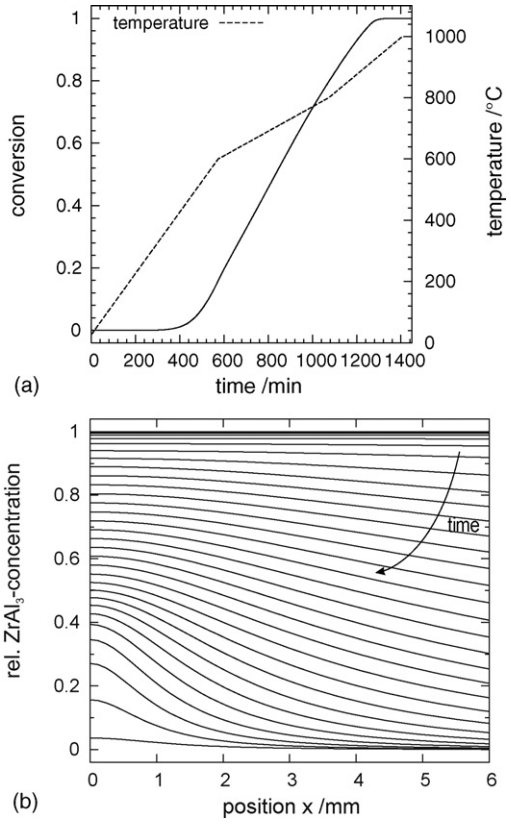

Fig. 6. Simulated TG curve (1 °C/min → 600 °C, 0.4 °C/min → 800 °C, 0.6 °C/min → 1000 °C) and conversion profiles for the 6 mm sample; the time steps between the conversion profiles are ∼33 min, respectively.

in the case of a diffusional limited process the heating cycle has to be modified to allow a uniform oxidation of the larger sample. As already mentioned previously, an effective heating cycle resulting in a constant weight gain rate includes several low linear heating rates giving sufficient time for a uniform reaction. This is demonstrated in Fig. 6 for the 6 mm sample, where three different low linear heating rates are incorporated in the heating cycle. Fig. 6(a) shows the simulated TG curve, whereas Fig. 6(b) shows the progression of the $ZrAl_3$ conversion profiles. As can be seen, only a slight gradient in the conversion profile is developed at the end of the reaction and the sample almost reacts

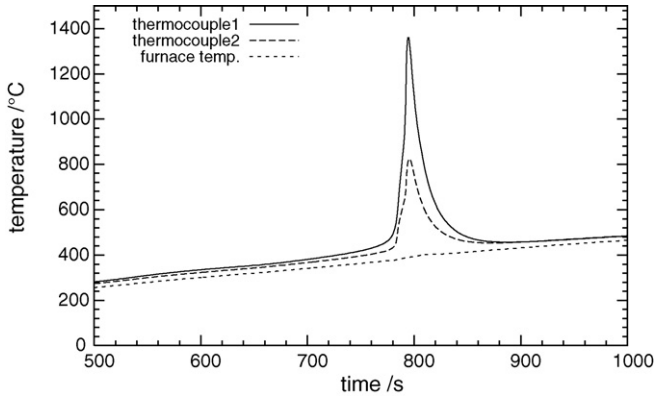

Fig. 7. Temperature measurements of a $ZrAl_3$ green body heated in a box furnance (∅ = 5.9 mm, ∼5 mm long, $\rho_{green} \approx 65\%$ TD; heating rate 20 °C/min; thermocouple 1: sample surface, thermocouple 2: near sample).

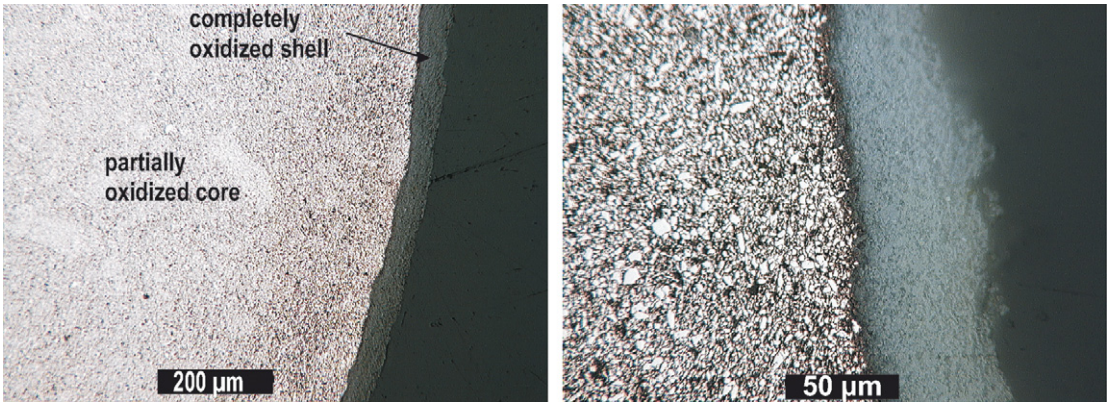

Fig. 8. Optical micrograph (cross-section) of a partially oxidized $ZrAl_3$ green compact ($\varnothing = 5.9$ mm, ~5 mm long, $\rho_{green} \approx 65\%$ TD; heating rate 20 °C/min in a box furnace).

uniformly. With this heating cycle a constant weight gain rate during the oxidation can be achieved.

4.4. Experimental validation

In this section, the predictive ability of the 1D reaction-diffusion model is demonstrated for the oxidation of $ZrAl_3$ compacts. Fig. 7 shows an example of the temperature measurements as a function of time. To demonstrate the high heat release of the exothermic oxidation reaction a relatively high heating rate of 20 °C/min was used. At a furnace temperature of about 400 °C there is an abrupt temperature rise of approximately 1350 °C. After this high temperature peak, the sample temperature drops down to the predetermined furnace temperature. This pronounced temperature peak is due to a surface-limited combustion reaction initiated by the reaction between the surface $ZrAl_3$ particles and the oxygen gas. A cross-section of such a sample is shown in Fig. 8. There are two distinct

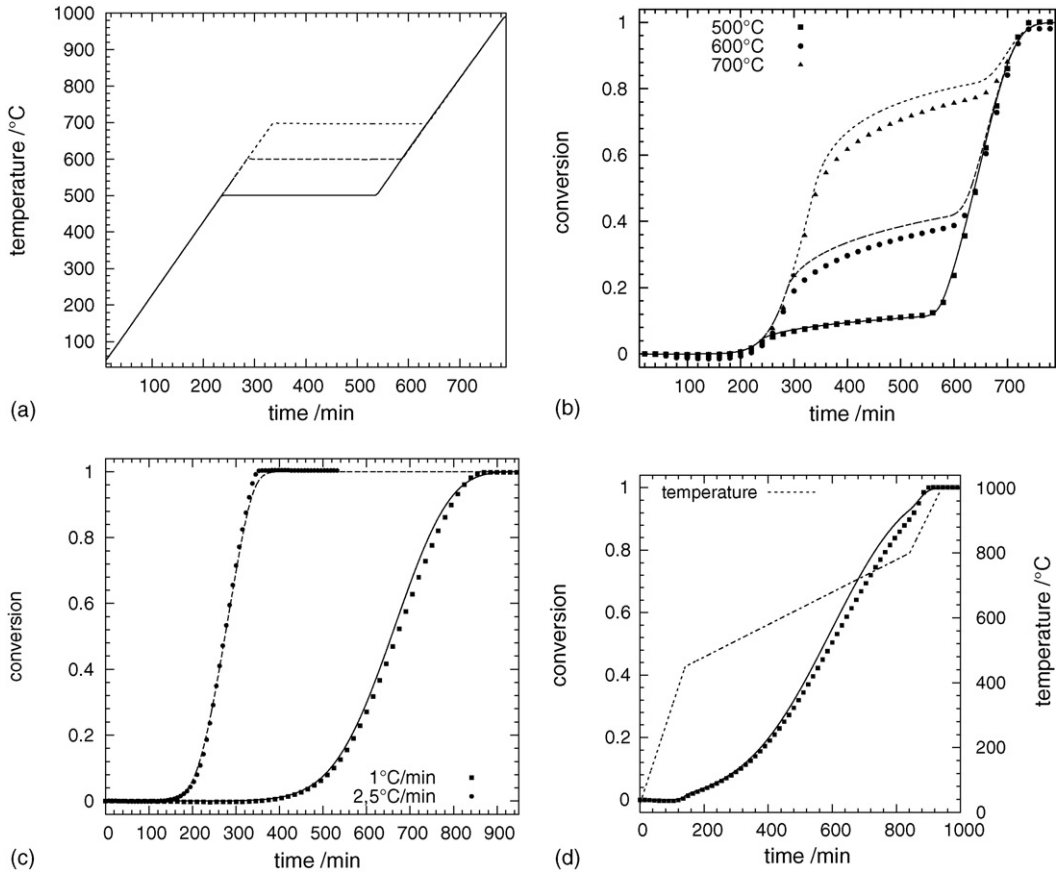

Fig. 9. Comparison of experimental and model-predicted TG curves of cylindrical green compacts ($\varnothing = 5.9$ mm and ~ 3.5 mm long). (a and b) Temperature profiles and corresponding conversion curves (isothermal hold time: 5 h with a heating rate of 2 °C/min), (c) linear heating rates $\beta = 1$ and 2.5 °C/min and (d) TG curves for following heating cycle: 3 °C/min → 450 °C, 0.5 °C/min → 800 °C, 2 °C/min → 1000 °C (lines: model-predicted; symbols: experimental).

regions: a partially oxidized core and a fully reacted shell of thickness of about 50 μm. The oxide scale consists of α-Al_2O_3, monoclinic and tetragonal ZrO_2 and has a relative dense structure which impedes further oxygen diffusion into the sample. The reaction interface is almost parallel to the sample surface, suggesting that the reaction is limited by the radial permeation of oxygen through the porous $ZrAl_3$ matrix. Similar behavior was reported by Anselmi-Tamburini et al. [29] for the combustion synthesis of ZrO_2 using metallic Zr powder.

To compare the predictions of the 1D finite difference model with the reaction behavior of real $ZrAl_3$ compacts, we performed thermogravimetric experiments of cylindrical samples. Due to the limitations of the sample holder of the thermal analyzer, only samples with about 6 mm in diameter could be investigated. For the calculations following parameter values were used: $L = 1.75$ mm, $k_g = 0.006$ m/s, $h = 15\ \mathrm{W/m^2\,K}$ and $\epsilon = 0.5$. The results of the thermogravimetric measurements together with the simulated data for different heating cycles are pesented in Fig. 9. As can be seen, the experimental data can be reproduced very well by the 1D reaction-diffusion model. However, the model overestimates the conversion degree to some extent. Possible explanations for this deviation are the one-dimensional approxiation of the reacting sample and the assumption of constant heat and mass transfer coefficients. It should also be mentioned that the samples reacted with linear heating rates of 5 and 10 °C/min were broken due to violent oxidation reactions. This is in accordance with the simulation results shown in Fig. 3(b), where high ΔT peaks are observed for these heating rates.

5. Conclusions

Reaction bonding techniques are usually based on highly exothermic gas–solid reactions. For this type of reactions process control is difficult to achieve. Therefore a mathematical model was developed, which is capable to describe the reaction bonding of alumina–zirconia composites based on the oxidation of the intermetallic compound $ZrAl_3$. This reaction-diffusion model takes into account the microkinetics at the powder particle level as well as the diffusion of oxygen through the porous $ZrAl_3$ green body. The numerical results indicate that the reaction behavior is very sensitive to the heat and mass transfer conditions and the heating cycle. Thermal runaway, i.e. surface-limited combustion, can occur when the heating rate is too high or the values of the heat loss parameters are too low. Experimental temperature measurements indicate that sample temperatures as high as 1350 °C are possible during thermal runaway. During oxidation of $ZrAl_3$ compacts the reaction can proceed in two different ways: (a) the rate limiting step is the chemical reaction of the powder particles. This results in an uniform oxidation of the sample; (b) the reaction becomes diffusion-limited. This is the case for larger green compacts, where the diffusion path lengths of oxygen are larger. A uniform reaction throughout the sample can be achieved with a heating cycle including a combination of different linear heating rates. The simulated data is in good agreement with the experimental thermogravimetric data. Therefore, the developed model can be used to plan heating schedules for reaction bonding of alumina–zirconia composites of different sizes. Further progress can be made by extending this work to more complex geometries such as any three-dimensional shape and incorporating possible changes of the microstructure or sintering effects.

References

[1] V. Hlavacek, J.A. Puszynski, Chemical engineering aspects of advanced ceramic materials, Ind. Eng. Chem. Res. 35 (1996) 349–377.
[2] V.D. Hennige, J. Haußelt, H.-J. Ritzhaupt-Kleissl, T. Windmann, Shrinkage-free $ZrSiO_4$-ceramics: Characterisation and applications, J. Eur. Ceram. Soc. 19 (1999) 2901–2908.
[3] H. Geßwein, J.R. Binder, H.-J. Ritzhaupt-Kleissl, J. Haußelt, Fabrication of net shape reaction bonded oxide ceramics, J. Eur. Ceram. Soc. 26 (2006) 697–702.
[4] R.J. Kematick, H.F. Franzen, Thermodynamic study of the zirconium–aluminum system, J. Solid State Chem. 54 (1984) 226–234.
[5] I. Barin, Thermochemical Data of Pure Substances, 3rd ed., VCH, 1995.
[6] W.B. Li, B.Q. Lei, T. Lindbäck, A kinetic model for reaction bonding process of silicon powder compact, J. Eur. Ceram. Soc. 17 (1997) 1119–1131.
[7] M. Maalmi, A. Varma, W. Strieder, Reaction-bonded silicon nitride synthesis: experiments and model, Chem. Eng. Sci. 53 (4) (1998) 679–689.
[8] E. Suvaci, G. Simkovich, G.L. Messing, The reaction-bonded aluminum oxide process. I. The effect of attrition milling on the solid state oxidation of aluminum powder, J. Am. Ceram. Soc. 83 (2) (2000) 299–305.
[9] S.P. Gaus, M.P. Harmer, H.M. Chan, H.S. Caram, Controlled firing of reaction-bonded aluminum oxide (RBAO) ceramic. Part I. Continuum-model predictions, J. Am. Ceram. Soc. 82 (4) (1999) 897–908.
[10] M.J. Watson, M.P. Harmer, H.M. Chan, H.S. Caram, Ignition phenomena and controlled firing of reaction-bonded aluminum oxide, Acta Mater. 49 (2001) 1095–1103.
[11] H. Geßwein, J.R. Binder, Thermokinetic study of the oxidation of $ZrAl_3$ powders, Thermochim. Acta 444 (2006) 6–12.
[12] M.R.A. El-Salam, M.H. Shehata, The numerical solution for reaction-diffusion combustion with fuel consumption, Appl. Math. Comput. 160 (2005) 423–435.
[13] A. Shah, A. Mcintosh, J. Brindley, J. Griffiths, M. Pourkashanian, The effect of oxygen starvation on ignition phenomena in a reactive solid containing a hot-spot, Combust. Theory Model. 7 (2003) 509–523.
[14] G.N. Mercer, R.O. Weber, B.F. Gray, S.D. Watt, Combustion pseudo-waves in a system with reactant consumption and heat loss, Math. Comp. Model. 24 (8) (1996) 29–38.
[15] G.N. Mercer, R.O. Weber, Combustion waves in two dimensions and their one-dimensional approximation, Combust. Theory Model. 1 (1997) 157–165.
[16] R.O. Weber, G.N. Mercer, H.S. Sidhu, B.F. Gray, Combustion waves for gases (Le = 1) and solids (Le → ∞), Proc. Roy. Soc. Lond. A 453 (1997) 1105–1118.
[17] G.N. Mercer, R.O. Weber, Radiation enhanced combustion wave speeds, Proc. Roy. Soc. Lond. A 453 (1997) 1543–1549.
[18] S. Gennari, F. Maglia, U. Anselmi-Tamburini, G. Spinolo, Self-propagating high-temperature synthesis of intermetallic compounds: a computer simulation approach to the chemical mechanisms, J. Phys. Chem. B 107 (2003) 732–738.
[19] S. Gennari, F. Maglia, U. Anselmi-Tamburini, G. Spinolo, SHS (self-sustained high temperature synthesis) of intermetallic compounds: effect of process parameters by computer simulation, Intermetallics 101 (2003) 1355–1359.
[20] H.P. Li, Influence of ignition parameters on micropyretic synthesis of NiAl compound, Mater. Sci. Eng. A 404 (2005) 146–152.
[21] M. Brown, D. Dollimore, A.K. Galwey, Reactions in the Solid State, vol. 22 of Comprehensive Chemical Kinetics, Elsevier, Amsterdam, 1980.
[22] S.F. Hulbert, Models for solid-state reactions in powdered compacts—a review, J. Br. Ceram. Soc. 6 (1969) 11–20.

[23] S. Wu, D. Holz, N. Claussen, Mechanisms and kinetics of reaction-bonded aluminum oxide ceramics, J. Am. Ceram. Soc. 76 (4) (1993) 970–980.
[24] G.N. Mercer, R.O. Weber, H.S. Sidhu, An oscillatory route to extinction for solid fuel combustion waves due to heat losses, Proc. Roy. Soc. Lond. A 454 (1998) 2015–2022.
[25] W.S. Janna, Engineering Heat Transfer, 2nd ed., CRC Press LLC, 2000.
[26] H.W. Dandekar, J.A. Puszynski, V. Hlavacek, Two-dimensional numerical study of cross-flow filtration combustion, AIChE J. 36 (11) (1990) 1160–1649.
[27] D.D. Smith, Numerical Solution of Partial Differential Equations Finite Difference Methods, 3rd ed., Oxford Applied Mathematics and Computing Science, Clarendon Press, Oxford, 1985.
[28] E. Hairer, G. Wanner, Solving Ordinary Differential Equations II. Stiff and Differential–Algebraic Problems, vol. 14 of Springer Series in Computation Mathematics, Springer-Verlag, Berlin, 1991.
[29] U. Anselmi-Tamburini, G. Spinolo, Z.A. Munir, Mechanistic observations on the combustion synthesis of pure and yttria-doped ZrO_2, J. Mater. Sci. Process. 1 (5) (1993) 323–333.